Bioorganic & Medicinal Chemistry 17 (2009) 7239–7247

Contents lists available at ScienceDirect

Bioorganic & Medicinal Chemistry

journal homepage: www.elsevier.com/locate/bmc

Synthesis and pharmacological exploitation of clioquinol-derived copper-binding apoptosis inducers triggering reactive oxygen species generation and MAPK pathway activation

Hui-Ling Chen [a], Chun-Yi Chang [b], Hsun-Tzu Lee [b], Hua-Hsuan Lin [b], Pei-Jung Lu [a], Chia-Ning Yang [c], Chung-Wai Shiau [d], Arthur Y. Shaw [b,*]

[a] Institute of Clinical Medicine, National Cheng Kung University, Tainan 701, Taiwan
[b] Department of Chemistry, Tamkang University, Tamsui 251, Taiwan
[c] Institute of Biotechnology, National University of Kaohsiung, Kaohsiung 700, Taiwan
[d] Institute of Biopharmaceutical Sciences, National Yang-Ming University, Taipei 112, Taiwan

ARTICLE INFO

Article history:
Received 10 July 2009
Revised 26 August 2009
Accepted 26 August 2009
Available online 1 September 2009

Keywords:
Clioquinol
Mannich-type reaction
Metal-binding property
Reactive oxygen species (ROS)
MAPK pathway activation

ABSTRACT

In the present study, we carried out Mannich-type reaction to synthesize clioquinol-derived 7-methyl-arylsulfonylpiperazine analogs with improved growth-inhibitory effects. **11** bearing 5-nitro group on the quinoline ring exhibited 26-fold more potent than that of clioquinol against HeLa cells with a GI_{50} value of 0.71 μM. In addition, **11** revealed synergistic effects on the growth inhibition of HeLa cells with GI_{50} values of 0.65, 0.25, and 0.06 μM in the presence of 1, 10, and 50 μM copper, respectively. Consistent to the clioquinol-mediated apoptosis, mechanistic study indicates that **9**- and **11**-induced growth inhibition is attributed to caspase-dependent pathway. Detection of reactive oxygen species in response to clioquinol, **9** and **11** confirmed that ROS was dramatically stimulated in the presence of copper and partially abolished upon treatment of 1 mM tempol. Further study indicated that **9**- and **11**-mediated induction of oxidative stress by ROS generation resulted in the activation MAPK pathway.

1. Introduction

Reactive oxygen species (ROS) are highly reactive molecules presenting radical and non-radical structure: superoxide anion, hydrogen peroxide, hydroxyl radical, and singlet oxygen. In the biological system, ROS are generated by enzymatic and non-enzymatic reactions which play a central role as second messengers in a number of signal transduction pathways, such as mitogen-activated protein kinases (MAPK), protein phosphatases, and transcription factors. The oxidative stress generally describes a condition in which cellular antioxidant defense mechanisms are insufficient to deactivate ROS, or excessive ROS are generated, or both. The maintenance of cellular redox balance is regulated by a powerful antioxidant system that inactivates ROS. It comprises of SOD, catalase, the glutathione system (glutathione, glutathione reductase, peroxidase, and transferase), the thioredoxin system (thioredoxins, thioredoxin peroxidase, and peroxiredoxins), vitamin E and C. The influence of cellular response to redox modulation is extensive and includes both proliferative and apoptotic pathways. Generally, low levels of ROS, particularly hydrogen peroxide, are mitogenic to promote cell proliferation, while medium levels result in either transient or permanent growth arrest. Redundant ROS eventually cause cell death through apoptotic or necrotic mechanisms.[1,2]

Clioquinol (5-chloro-7-iodo-8-hydoxyquinoline) was widely used as an antibiotic for the treatment of diarrhea and skin infection (Fig. 1). The metal-binding properties of clioquinol led to its application in a mouse model of Alzheimer's disease via the reduction or prevention of amyloid plaque accumulation in the brain. It was then moved to clinical trials for patients with Alzheimer's disease.[3,4] On the other hand, clioquinol also exhibited growth-inhibitory effect against a panel of cancer cell lines. The mechanistic study of clioquinol-induced apoptosis revealed that clioquinol served as an ionophore that elevated levels of intracellular zinc for cytotoxic potentiation. The apoptosis induced by clioquinol was attributed to the activation of caspase-dependent pathways and inhibition of proteasome activity.[5–7]

In the present study we sought to synthesize clioquinol-derived apoptosis inducers by means of Mannich-type reaction with aim to examine their growth-inhibitory effects against carcinoma cell lines. We further provided evidence that apoptosis induced by clioquinol and its analogs was potentiated by copper ion through reactive oxygen species generation.

* Corresponding author. Tel.: +886 2 2621 5656x2842; fax: +886 2 2620 9924.
E-mail address: shaw299@mail.tku.edu.tw (A.Y. Shaw).

0968-0896/$ - see front matter © 2009 Elsevier Ltd. All rights reserved.
doi:10.1016/j.bmc.2009.08.054

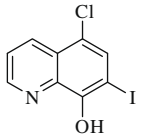

Clioquinol

Figure 1. Chemical structure of clioquinol.

2. Results and discussion

2.1. Synthesis of Mannich bases

Herein, we take advantage of the three-component one-pot synthesis of Mannich-type reaction as shown in Scheme 1. In general, the mixture of 8-hydroxyquinoline (**1**), 1-naphthol (**2**), or 5-nitro-8-hydroxyquinoline (**3**), along with formaldehyde and corresponding secondary amines was stirred in ethanol at reflux for 16 h to afford Mannich bases **7**–**11**.[8–10]

2.2. Growth inhibition of clioquinol and Mannich bases against carcinoma cell lines

The evaluation of growth-inhibitory activity of clioquinol and Mannich bases **7**–**11** was examined on a panel of carcinoma cell lines, including HeLa (cervical epithelioid carcinoma cell), BT483 (mammary gland adenocarcinoma cell), SKHep (hepatocellular carcinoma cell), and CE81T (esophageal carcinoma cell). The MTT (3-[4,5-dimethylthiazol-2-yl]-2,5-diphenyltetrazolium bromide) assay was employed for growth inhibition studies and the GI_{50} values are summarized in Table 1. The tested compound concentration causing a 50% cell growth inhibition (GI_{50}) was determined by interpolation from dose-response curves.

Among four carcinoma cell lines, HeLa cells were most sensitive in response to tested compounds on growth inhibition. As shown, exposure of HeLa cells to clioquinol and Mannich bases **7**–**11** in 10% FBS-supplemented DMEM medium for 48 h resulted in the growth inhibition with a range of GI_{50} values between 0.7 and 25.5 μM. Clioquinol as a positive control showed a moderate growth-inhibitory effect on HeLa cells with a GI_{50} value of 18.6 μM. An appreciable growth inhibition on HeLa cells was observed while introducing 7-methyl-piperidine (**7**, GI_{50}, 14.5 μM) and 7-methyl-arylsulfonylpiperazine moieties (**9**, GI_{50}, 6.8 μM) on the 8-hydroxyquinoline scaffold. In particular, **11** bearing 5-nitro group on the quinoline ring exhibited 26-, 5-, and 4-fold more potent than that of clioquinol against HeLa (GI_{50}, 0.7 vs 18.6 μM), BT483 (GI_{50}, 1.9 vs 10.2 μM) and CE81T (GI_{50}, 5.9 vs 23.4 μM) cells, respectively. Together, these results indicate that structural optimization could be achieved by the appropriate elongation of 8-hydroxyquinoline and substitution on quinoline ring. On the contrary, 1-naphthol-bearing **8** and **10** exhibited decreased growth inhibition against HeLa cells with GI_{50} values of 25.5 and 38.6 μM, respectively. Moreover, as high as 40 μM treatment of **8** and **10**, no appreciable growth-inhibitory effect was observed on the rest of BT483, SKHep, and CE81T cell lines, indicating that 8-hydroxyquinoline skeleton plays a crucial role for growth-inhibitory activity.

Table 1
Growth inhibition of clioquinol (**CQ**) and Mannich bases **7–11** against carcinoma cell lines

Entry	GI_{50}[a] (μM)			
	HeLA	BT483	SKHep	CE81T
CQ	18.6 ± 2.4	10.2 ± 0.6	9.5 ± 0.6	23.4 ± 2.5
7	14.5 ± 1.7	26.9 ± 3.2	16.6 ± 2.5	16.7 ± 0.8
8	25.5 ± 2.7	ND[b]	ND	ND
9	6.8 ± 1.1	10.7 ± 2.6	14.6 ± 3.6	5.6 ± 1.8
10	38.6 ± 4.0	ND	ND	ND
11	0.71 ± 0.15	1.9 ± 0.1	14.6 ± 0.6	5.9 ± 0.5

[a] GI_{50} values are presented as the mean ± SEM (standard error of the mean) from four to six separated experiments.
[b] ND indicated that no appreciable growth inhibition was observed upon treatment of maximal concentration at 40 μM.

2.3. Enhancement of growth inhibition of clioquinol and Mannich bases against HeLa cells in the presence of metal ion

Similar to the results demonstrated in the literature, the metal-binding properties of clioquinol enhanced its growth-inhibitory effect on HeLa cells in the presence of both copper and zinc. As shown in Table 2, both copper and zinc potentiated clioquinol-induced growth inhibition toward HeLa cells in a dose-dependent manner. Meanwhile, **7**, **9**, and **11** exhibited significantly synergistic effects on growth inhibition in the presence of 50 μM copper with GI_{50} values of 0.35, 0.27, and 0.06 μM, respectively, all of which exhibited more potent than that of clioquinol with a GI_{50} of 4.4 μM. However, the synergistic effect with zinc was not as obvious as that of copper. This discrepancy might be attributed to the distinct redox sensitivity of specific metal ions that counts for the stability of intracellular redox balance. On the other hand, the counterparts **8** and **10** did not show significant growth inhibition in the presence of both copper and zinc. These findings clearly confirmed the metal-binding property of 8-hydroxyquinoline skeleton in clioquinol, **7**, **9**, and **11**.

2.4. Mannich bases induce apoptosis through caspase-dependent pathways

To determine whether induction of apoptosis mediated by clioquinol-derived Mannich bases is similar to that of clioquinol in the literature,[5] analysis of HeLa cells was examined after treatment of **9** for 24 and 48 h. According to the flow cytometric analysis shown

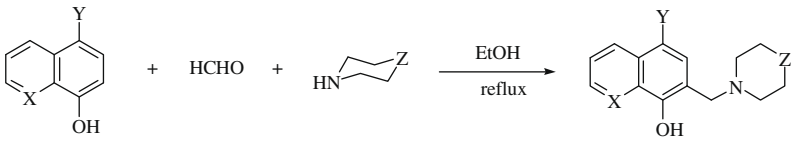

1 X = N, Y = H
2 X = CH, Y = H
3 X = N, Y = NO_2

4 Z = CH_2
5 Z = NSO_2Ph
6 Z = $NSO_2C_6H_4(4\text{-}CH_3)$

7 X = N, Y = H, Z = CH_2
8 X = CH, Y = H, Z = CH_2
9 X = N, Y = H, Z = NSO_2Ph
10 X = CH, Y = H, Z = NSO_2Ph
11 X = N, Y= NO_2, Z = $NSO_2C_6H_4(4\text{-}CH_3)$

Scheme 1.

Table 2
Growth inhibition of clioquinol (CQ) and Mannich bases **7–11** against HeLa cells in the presence of metal ion

Entry	GI_{50}[a] (μM)					
	$CuCl_2$ (μM)				$ZnCl_2$ (μM)	
	0	1	10	50	50	100
CQ	18.6 ± 2.4	6.1 ± 1.8	5.3 ± 1.2	4.4 ± 0.9	5.6 ± 0.8	2.1 ± 0.8
7	14.5 ± 1.7	3.0 ± 0.9	0.58 ± 0.09	0.35 ± 0.08	8.5 ± 1.9	12.9 ± 1.6
8	25.5 ± 2.7	30.7 ± 3.8	22.8 ± 4.2	48.8 ± 4.5	34.0 ± 5.9	44.5 ± 4.8
9	6.8 ± 1.1	2.5 ± 0.8	0.31 ± 0.07	0.27 ± 0.06	7.5 ± 1.6	7.3 ± 2.4
10	38.6 ± 4.0	40.1 ± 5.2	28.4 ± 3.4	22.6 ± 2.4	29.7 ± 4.8	20.1 ± 4.3
11	0.71 ± 0.15	0.65 ± 0.12	0.25 ± 0.07	0.06 ± 0.05	0.48 ± 0.09	0.26 ± 0.05

[a] GI_{50} values are presented as the mean ± SEM (standard error of the mean) from four to six separated experiments.

in Figure 2A, HeLa cells exposed to **9** for 24 h treatment was found to exhibit sub-G1 phase arrest in a dose-dependent manner, suggesting that growth inhibition mediated by 8-hydroxyquinoline analogs resulted in DNA fragmentation. Moreover, western blot of cytosolic extracts prepared from **9**-treated cells revealed cleavage of the 116-kDa protein poly(ADP-ribose) polymerase (PARP) and generation of the 89-kDa fragment. The appearance of a 85-kDa fragment coincided with the activation of caspase-3, as shown by the reduced level of the 32-kDa proenzyme and the increased level of the 17/19-kDa cleaved caspase-3 (Fig. 2B). The activation of the upstream caspase-9 was also observed with the reduced level of the 45-kDa proenzyme, indicating the mitochondrial apoptotic pathway was involved. Taken together, the **9**-mediated apoptotic effects are in agreement with the findings in clioquinol-mediated apoptosis through the caspase-dependent pathway. In light of growth-inhibitory activity of Mannich bases enhanced through metal-binding property, we demonstrated the synergistic effect of apoptosis in the presence of copper.

As shown in Figure 3, exposure of HeLa cells to **9** at 3 μM and **11** at 1 μM in the presence of 10 μM copper enhanced sub-G1 phase arrest rising from 7.9% and 6.8% to 29.8% and 17.5%, respectively. The sub-G1 phase arrest was reduced upon treatment of caspase inhibitor z-VAD at 10 μM (Fig. 3L). Moreover, accumulation of sub-G1 phase cells diminished upon treatment of 1 mM tempol (Fig. 3K), a cell membrane-permeable radical scavenger, which prompted us to examine reactive oxygen species (ROS) formation.

2.5. Clioquinol and Mannich bases trigger reactive oxygen species (ROS) generation

Clioquinol is a metal-binding agent that binds metal ions extracellularly and transports them into the cells. In addition, copper ion is a redox-active metal that may be more redox active as complexed with some metal-binding agents, which may result in the generation of reactive oxygen species and exhibit cytotoxicty.[11,12] As shown in Figure 4, the production of ROS was dramatically stimulated upon treatment of CQ at 10 μM, **7** and **9** at 3 μM, and **11** at 1 μM in the presence of indicated concentrations of copper ion. Moreover, ROS generation was partially abolished by the addition of 1 mM tempol. Consequently, modulation of ROS production is in accordance with our flow cytometric data in which the sub-G1 phase arrest is reduced upon co-treatment of 1 mM tempol. Taken together, we conclude that the apoptosis-inducing effect mediated by clioquinol and Mannich bases is, in part, through the generation of reactive oxygen species.

2.6. 8-Hydroxyquinoline-induced activation of mitogen-activated protein kinase (MAPK) pathway

MAPK is one of the most common signaling pathways activated in response to various cellular stimuli such as oxidative stress. Three major MAPK subfamilies have been identified: extracellular signal-regulated kinase (ERK), p38 MAPK, and c-Jun N-terminal kinase (JNK). In addition, activation of MAPK subfamilies has been shown to be important in the oxidative stress-mediated cell death. Therefore, as indicated in Figure 5A, we showed that upon exposure of HeLa cells to 3 μM **9** in the presence of 10 μM copper, JNK, p38 and ERK were dramatically activated in a time-dependent manner in response to oxidative stress induced by **9**. In addition, the activation of MAPK pathway was reversed upon treatment of tempol and that without copper treatment. Moreover, the activation of MAPK pathways as well as caspase-3 and PARP were also observed upon the long-term treatment of HeLa cells with **11** at 1 μM for 24–48 h in the presence of 10 μM copper as shown in Figure 5B.

3. Conclusions

In summary, the present study we take advantage of the practical Mannich-type reaction to synthesize a new class of clioquinol-derived 7-methyl-arylsulfonylpiperazine analogs with improved growth-inhibitory effects. In particular, analog **11** bearing 5-nitro group on the quinoline ring exhibited 26-fold more potent than the parent compound clioquinol against HeLa cells. In the presence of 50 μM copper ion, **11** revealed significantly synergistic effects on the growth inhibition of HeLa cells with a GI_{50} value of 0.06 μM. These results suggest that clioquinol containing 8-hydroxyquinoline scaffold is amenable for structural modifications with improved growth-inhibitory activity independent of metal-binding property. The mechanistic study on the growth inhibition of HeLa cell mediated by Mannich bases agreed with clioquinol-induced caspase-dependent apoptotic pathway. The well-known redox property of copper ion enables its cytotoxic when present in excess of cellular requirements. For example, the intracellular cytotoxic effects associated with copper exposure are consistent with oxidative damage of lipids, proteins, and nucleic acids. Current study shows that clioquinol and Mannich bases trigger potential stimulation of reactive oxygen species upon co-treatment of copper ion. In addition, Western blot analysis reveals that upon treatment of **11** in the presence of copper ion phosphorylated histone H2AX in a time-dependent manner (data not shown), indicating the response of DNA damage to **11**-Cu-induced oxidative stress. Detection of reactive oxygen species in response to clioquinol, **7**, **9**, and **11** also confirmed that ROS could be dramatically stimulated in the presence of copper ion. Upon treatment of 1 mM tempol, ROS production was partially abolished which was corresponding to the minimized sub-G1 phase arrest in the flow cytometric analysis. We conclude that consecutive activation of MAPK pathway was accompanied by ROS production that leads to the oxidative-stressed microenvironment and eventually executed programmed cell death.

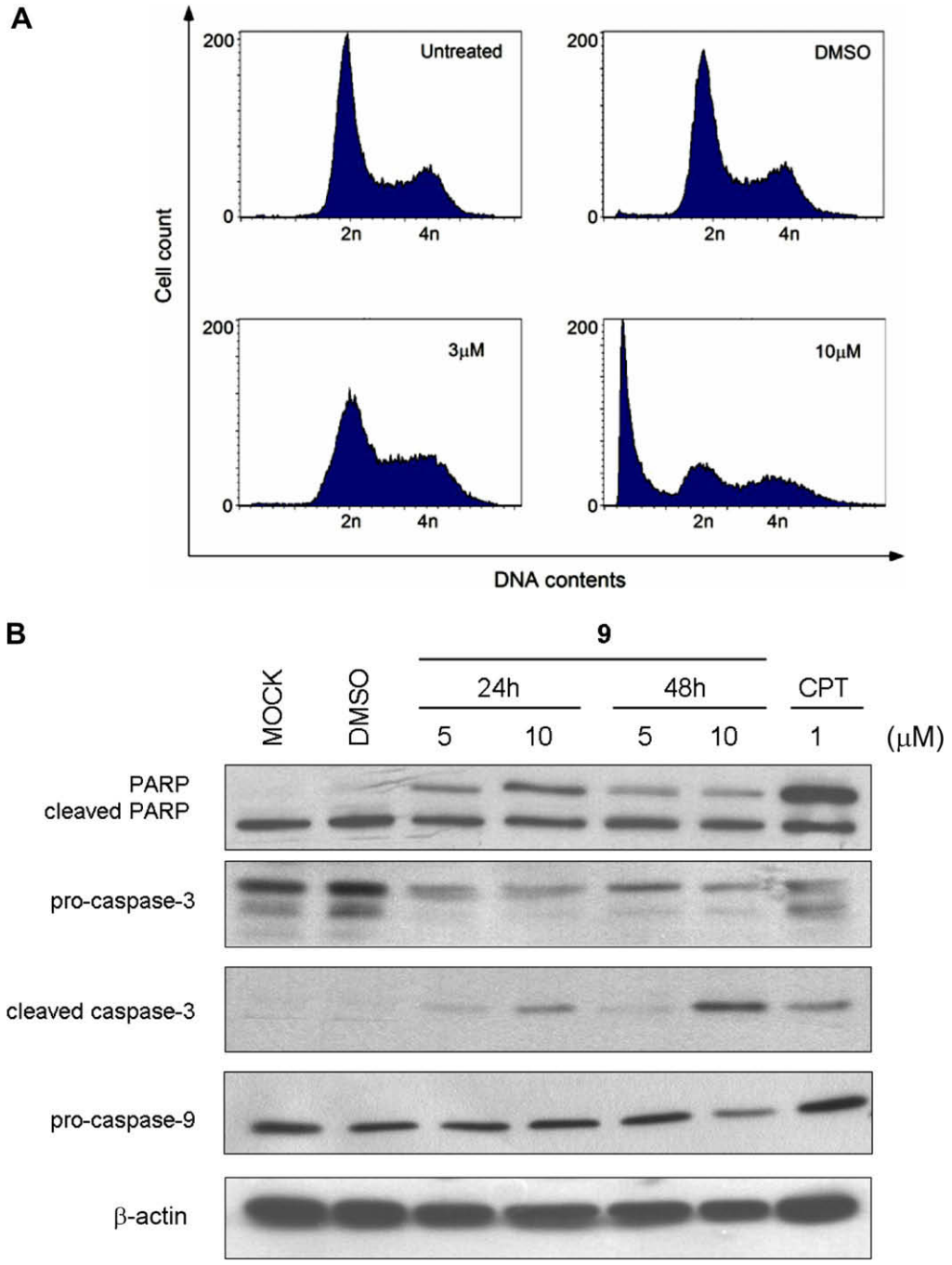

Figure 2. Induction of apoptosis in HeLa cells by **9**. (A) Untreated HeLa cells were taken as blank group. Cells were treated with 0.5% DMSO as the control. Cells were harvested after 24 h exposure to 3 and 10 μM of **9** and followed by fixation, propidium iodide staining prior to the flow cytometric analysis. Sub-G1 phase indicated the DNA fragmentation and cell death. (B) Induction of poly(ADP-ribose) polymerase (PARP) cleavage by **9** at the indicated concentrations after 24 and 48 h of treatment. PARP proteolysis to the apoptosis-specific 85-kDa fragment was monitored by western blotting. The appearance of a 89-kDa fragment coincided with the activation of caspase-3, as shown by the reduced level of the 32-kDa proenzyme and the increased level of the 17/19-kDa cleaved caspase-3. The activation of the upstream caspase-9 was also observed with the reduced level of the 45-kDa proenzyme, indicating the mitochondrial apoptotic pathway was involved. CPT as the positive control.

4. Materials and methods

4.1. Synthesis

Chemical reagents and organic solvents were purchased from TCI and Alfa Aesar unless otherwise mentioned. Melting points were determined by Fargo MP-2D. Nuclear magnetic resonance spectra (^{1}H and ^{13}C NMR) were measured on a Bruker AC-300 instrument. Chemical shifts (δ) are reported in ppm relative to the TMS peak. Mass spectra were obtained by FAB on a Jeol JMS-700 instrument. Flash column chromatography was performed with silica gel (230–400 mesh). Elemental Analysis was carried out on a Heraeus VarioEL-III C, H, N analyzer.

4.1.1. The general experimental procedure

To a solution of 8-hydroxyquinoline or 1-naphthnol (1.05 mmol) and paraformaldehyde (36 mg, 1.26 mmol) in dry ethanol (8 mL) was added the appropriate secondary amine (1.26 mmol) at room

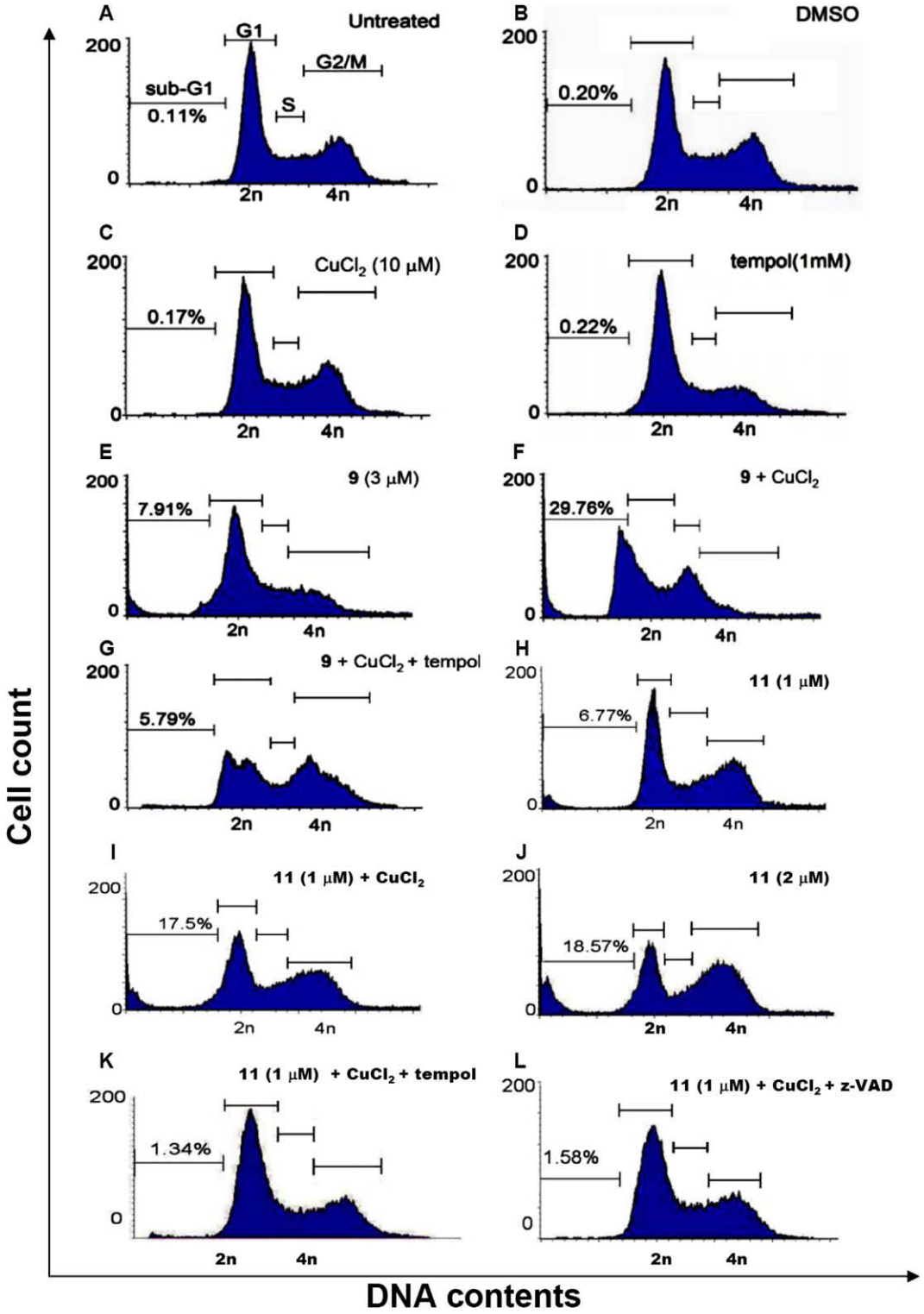

Figure 3. Flow cytometric analysis of HeLa cells. Cells were harvested after 24 h treatment and followed by fixation, propidium iodide staining prior to the flow cytometric analysis. Sub-G1 phase indicated the DNA fragmentation and cell death. Exposure of HeLa cells to **9** at 3 μM and **11** at 1 μM in the presence of 10 μM copper enhanced sub-G1 phase arrest increasing from 7.9% and 6.8% to 29.8% and 17.5%, respectively. The sub-G1 phase arrest was reduced upon treatment of tempol (Fig. 3K) and z-VAD (Fig. 3L). (A) Untreated HeLa cells were taken as blank group; (B) cells were treated with 0.5% DMSO as the control; (C) $CuCl_2$ 10 μM; (D) tempol 1 mM; (E) treatment of **9** at 3 μM; (F) treatment of **9** at 3 μM in the presence of $CuCl_2$ 10 μM; (G) treatment of **9** at 3 μM in the presence of $CuCl_2$ at 10 μM and temopl at 1 mM; (H) treatment of **11** at 1 μM; (I) treatment of **11** at 1 μM in the presence of $CuCl_2$ at 10 μM; (J) treatment of **11** at 2 μM; (K) treatment of **11** at 1 μM in the presence of $CuCl_2$ at 10 μM and temopl at 1 mM; (L) treatment of **11** at 1 μM in the presence of $CuCl_2$ at 10 μM and z-VAD at 10 μM.

temperature. The resulting mixture was heated at reflux for 18–22 h. The solvent was removed in vacuo and the crude product was purified by flash chromatography and/or recrystallization.

4.1.2. 7-(Piperidin-1-ylmethyl)quinolin-8-ol (7)

Mp 115–117 °C. (lit.[8] 114–117 °C). ^{1}H NMR (300 MHz, $CDCl_3$) δ 1.45 (d, J = 4.1 Hz, 2H), 1.58–1.65 (m, 4H), 2.52 (br s, 4H), 3.78 (d,

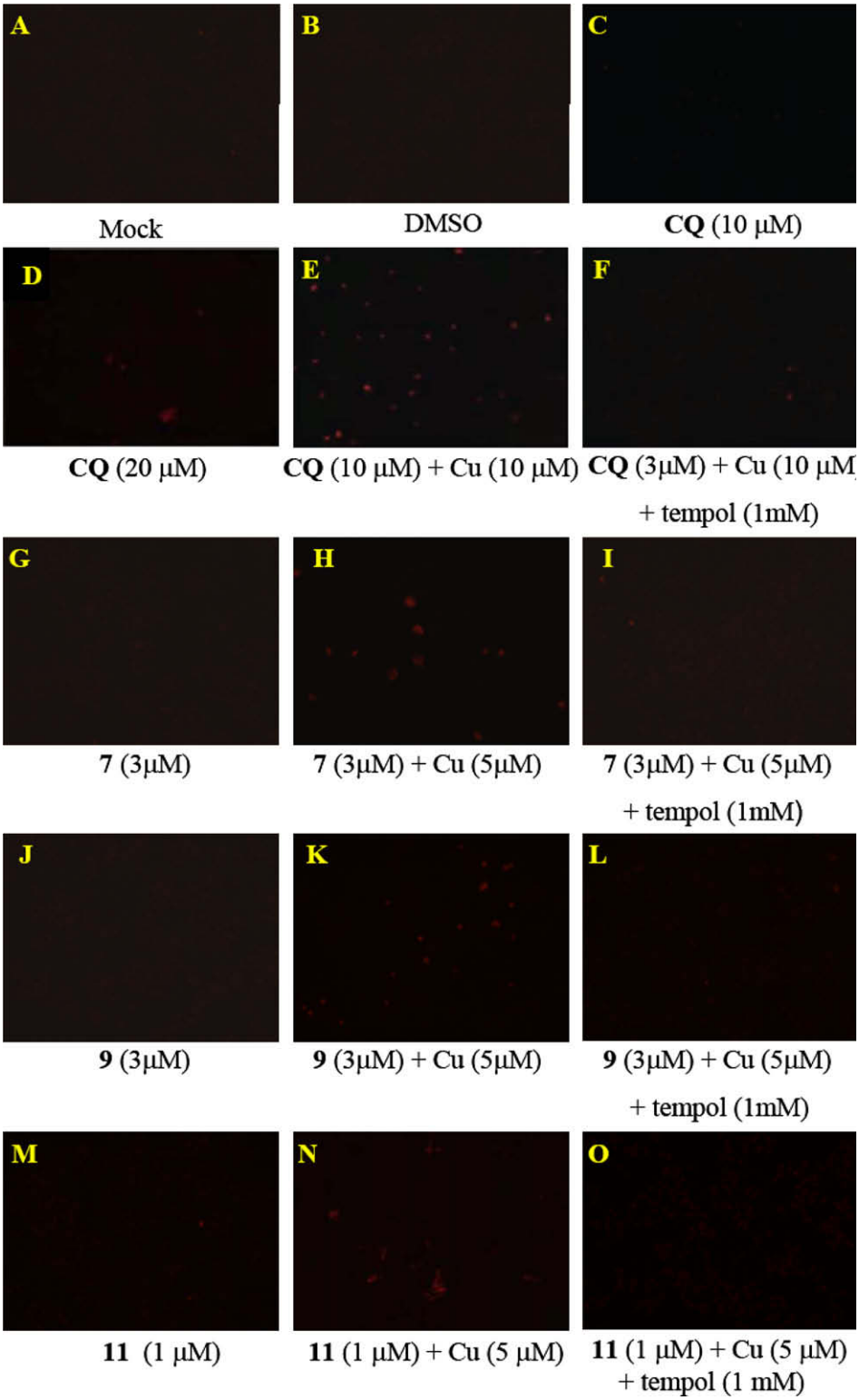

Figure 4. Reactive oxygen species detection. The production of ROS in HeLa cells was observed for 1 h treatment with **CQ**, **7**, **9**, and **11** at indicated concentrations. Generation of ROS could be partially abolished by the treatment of 1 mM tempol. (A) Untreated HeLa cells were taken as blank group; (B) Cells were treated with 0.5% DMSO as the control; (C) treatment of **CQ** at 10 μM; (D) treatment of **CQ** at 10 μM; (E) treatment of **CQ** at 10 μM in the presence of $CuCl_2$ 10 μM; (F) treatment of **CQ** at 10 μM in the presence of $CuCl_2$ 10 μM and tempol 1 mM; (G) treatment at **7** at 3 μM; (H) treatment of **7** at 3 μM in the presence of $CuCl_2$ 5 μM; (I) treatment of **7** at 3 μM in the presence of $CuCl_2$ 5 μM and tempol 1 mM; (J) treatment at **9** at 3 μM; (K) treatment of **9** at 3 μM in the presence of $CuCl_2$ 5 μM; (L) treatment of **9** at 3 μM in the presence of $CuCl_2$ 5 μM and tempol 1 mM; (M) treatment at **11** at 1 μM; (N) treatment of **11** at 1 μM in the presence of $CuCl_2$ 5 μM; (O) treatment of **11** at 3 μM in the presence of $CuCl_2$ 5 μM and tempol 1 mM.

J = 4.1 Hz, 2H), 7.10 (d, *J* = 8.3 Hz, 1H), 7.16 (d, *J* = 8.3 Hz, 1H), 7.26–7.30 (m, 1H), 7.97–8.01 (dd, *J* = 10.0 Hz, *J* = 6.6 Hz, 1H), 8.82–8.83 (dd, *J* = 5.8 Hz, *J* = 2.5 Hz, 1H) ppm. ^{13}C NMR (75 MHz, $CDCl_3$) δ 24.0, 25.9, 54.1, 61.8, 117.1, 118.0, 121.1, 127.3, 128.5, 135.6,

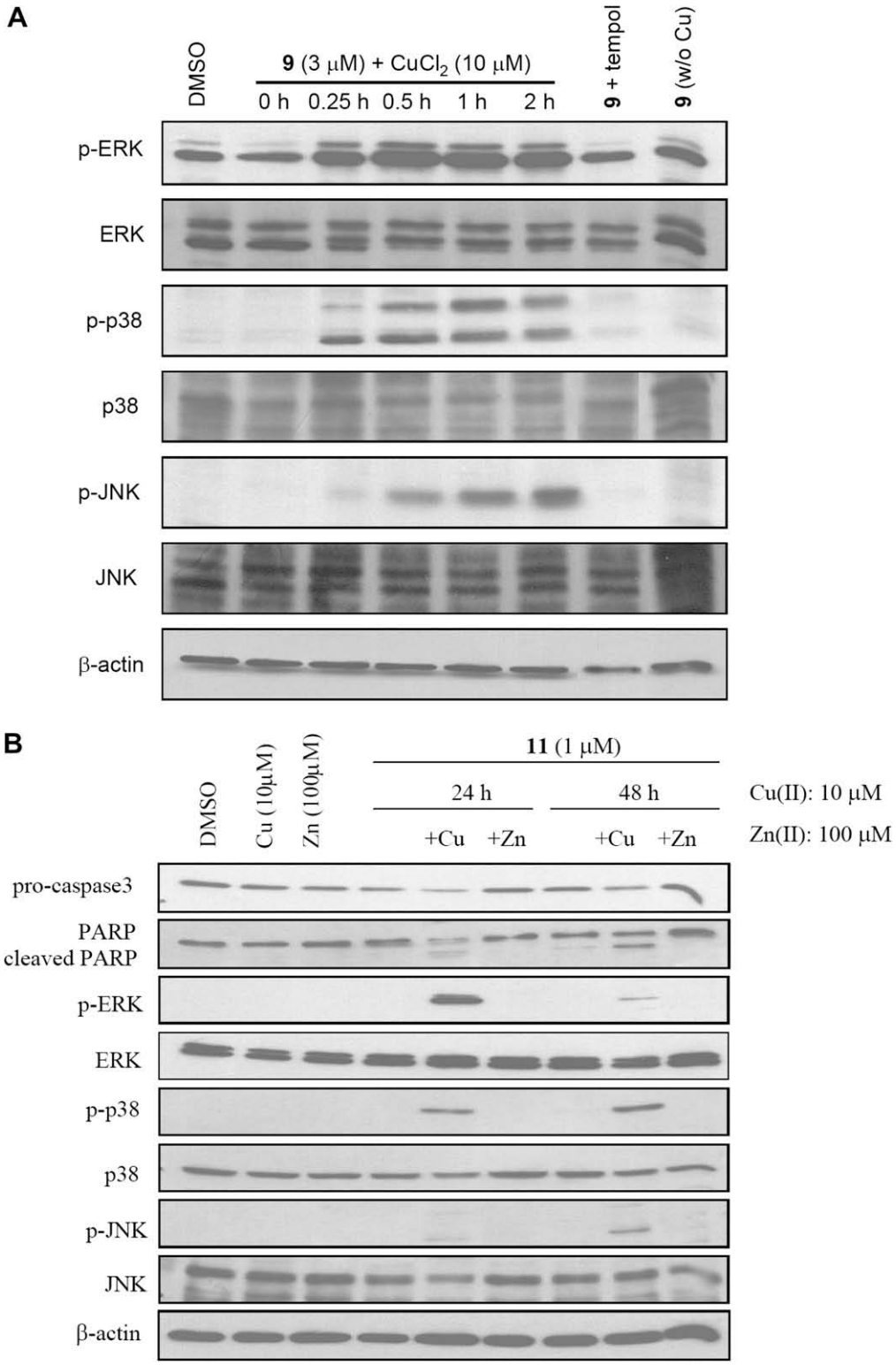

Figure 5. The activation of mitogen-activated protein kinase (MAPK) pathway mediated by Mannich bases **9** and **11**. (A) The phosphorylation of ERK, p38 and JNK was observed upon exposure of HeLa cells to **9** at 3 μM in the presence of $CuCl_2$ (10 μM) within 2 h treatment. In addition, the activation of MAPK pathway was reversed upon treatment of tempol and without copper treatment. (B) Cleavage of pro-caspase-3, poly(ADP-ribose) polymerase (PARP) and the phosphorylation of ERK, p38, and JNK were observed upon exposure of HeLa cells to **11** at 1 μM in the presence of $CuCl_2$ (10 μM) after 24 and 48 h treatment.

139.5, 149.0, 153.9 ppm. HRMS $(M+1)^+$ calcd for $C_{15}H_{19}N_2O$ 243.1497; found 243.1500. Anal. Calcd for $C_{15}H_{19}N_2O$: C, 74.35; H, 7.49; N, 11.56. Found: C, 74.10; H, 7.41; N, 11.46.

4.1.3. 2-(Piperidin-1-ylmethyl)naphthalen-1-ol (8)

Mp 133–135 °C. (lit.[10] 133.5–134.5 °C). ^1H NMR (300 MHz, $CDCl_3$) δ 1.53 (br s, 2H), 1.62–1.72 (m, 4H), 2.59 (br s, 4H), 3.82

(s, 2H), 7.07 (d, J = 8.3 Hz, 1H), 7.28 (d, J = 8.3 Hz, 1H), 7.40–7.48 (m, 2H), 7.73–7.78 (m, 1H), 8.23–8.28 (m, 1H) ppm. ^{13}C NMR (75 MHz, $CDCl_3$) δ 24.2, 26.0, 54.1, 62.4, 114.0, 118.2, 122.2, 124.9, 125.1, 126.0, 126.7, 127.5, 134.0, 153.9 ppm. HRMS $(M)^+$ calcd for $C_{16}H_{19}NO$ 241.1467; found 241.1465. Anal. Calcd for $C_{16}H_{19}NO$: C, 79.63; H, 7.94; N, 5.80. Found: C, 79.15; H, 7.91; N, 5.76.

4.1.4. 7-((4-(Phenylsulfonyl)piperazin-1-yl)methyl)quinolin-8-ol (9)

Mp 201–203 °C. ^{1}H NMR (300 MHz, $CDCl_3$) δ 2.69 (t, J = 4.9 Hz, 4H), 3.09 (br s, 4H), 3.85 (s, 2H), 7.24 (d, J = 5.4 Hz, 2H), 7.37 (dd, J = 10.5, 5.9 Hz, 1H), 7.50–7.56 (m, 2H), 7.59–7.64 (m, 1H), 7.72–7.75 (m, 2H), 8.07 (dd, J = 10.5 Hz, 1H), 8.79 (dd, J = 5.9 Hz, 1H) ppm. ^{13}C NMR (75 MHz, $CDCl_3$) δ 46.3, 52.0, 59.0, 117.6, 117.8, 121.7, 127.9, 128.4, 129.3, 133.3, 135.4, 135.9, 139.0, 148.9, 152.2 ppm. HRMS $(M)^+$ calcd for $C_{20}H_{21}N_3O_3S$ 383.1304; found 383.1304. Anal. Calcd for $C_{20}H_{21}N_3O_3S$: C, 62.64; H, 5.52; N, 10.96. Found: C, 62.56; H, 5.53; N, 10.85.

4.1.5. 2-((4-(Phenylsulfonyl)piperazin-1-yl)methyl)naphthalen-1-ol (10)

Mp 125.5–126.5 °C. ^{1}H NMR (300 MHz, CDCl3) δ 2.71 (br s, 4H), 3.11 (br s, 4H), 3.85 (s, 2H), 7.05 (d, J = 8.4 Hz, 1H), 7.29 (d, J = 8.3 Hz, 1H), 7.43 (t, J = 3.8 Hz, 2H), 7.57 (d, J =7.9 Hz, 2H), 7.65 (d, J = 7.0 Hz, 1H), 7.73–7.77 (m, 3H), 8.11 (t, J = 6.9 Hz, 1H) ppm. ^{13}C NMR (75 MHz, $CDCl_3$) δ 46.1, 51.9, 61.3, 113.0, 119.0, 122.4, 125.1, 126.4, 126.7, 127.6, 127.7, 127.9, 129.5, 133.4, 134.2, 135.7, 153.0 ppm. HRMS $(M)^+$ calcd for $C_{21}H_{22}N_2O_3S$ 382.1351; found 382.1350. Anal. Calcd for $C_{21}H_{22}N_2O_3S$: C, 65.95; H, 5.80; N, 7.32. Found: C, 65.56; H, 5.63; N, 7.81.

4.1.6. 5-Nitro-7-((4-tosylpiperazin-1-yl)methyl)quinolin-8-ol (11)

Mp 135.5–136.5 °C. ^{1}H NMR (300 MHz, $CDCl_3$) δ 2.46 (s, 3H), 2.72 (t, J = 4.8 Hz, 4H), 3.08 (t, J = 4.8 Hz, 4H), 3.89 (s, 2H), 7.35 (d, J = 8.2 Hz, 2H), 7.63 (d, J = 8.2 Hz, 2H), 7.67 (m, 1H), 8.45 (s, 1H), 8.91 (m, 1H), 9.25 (m, 1H) ppm. ^{13}C NMR (75 MHz, $CDCl_3$) δ 21.7, 46.1, 52.0, 57.4, 116.6, 122.2, 124.9, 127.9, 129.0, 130.0, 132.0, 133.2, 135.9, 137.8, 144.2, 149.6, 158.5 ppm. HRMS $(M)^+$ calcd for $C_{21}H_{22}N_4O_5S$ 442.1311; found 442.1335. Anal. Calcd for $C_{21}H_{22}N_4O_5S$: C, 57.00; H, 5.01; N, 12.66. Found: C, 56.45; H, 5.28; N, 12.55.

4.2. Cell culture

Cancer cells were purchased from Bioresource Collection and Research Center in Taiwan. Each cell line was maintained in the standard medium and grown as a monolayer in Dulbecco's Modified Eagle Medium (DMEM) containing 10% fetal bovine serum, 2 mM glutamine, 100 units/ml penicillin, and 100 g/ml streptomycin. Cultures were maintained at 37 °C with 5% CO_2 in a humidified atmosphere.

4.3. MTT assay for cell viability

Cells were plated in 96-well microtiter plates at a density of 5×10^3/well and incubated for 24 h. After that, cells were treated with vehicle alone (control) or compounds (drugs were dissolved in DMSO previously) at the concentrations indicated. Treated cells were further incubated for 48 h. Cell survival is expressed as percentage of control cell growth. The 3-[4,5-dimethylthiazol-2-yl]-2,5-diphenyltetrazolium bromide (MTT, 2 mg/mL) dye reduction assay in 96-well microplates was used. The assay is dependent on the reduction of MTT by mitochondrial dehydrogenases of viable cell to a blue formazan product, which come be measured spectrophotometrically. Tumor cells were incubated in each well with serial dilutions of the tested compounds. After 2 days of incubation (37 °C, 5% CO_2 in a humid atmosphere) 100 μL of MTT (2 mg/mL in PBS) was added to each well and the plate was incubated for a further 2 h (37 °C). The resulting formazan was dissolved in 100 μL DMSO and read at 570 nm. The percentage of growth inhibition was calculated by the following equation: percentage growth inhibition = $(1 - At/Ac) \times 100$, where At and Ac represent the absorbance in treated and control cultures, respectively. The drug concentration causing a 50% cell growth inhibition (GI_{50}) was determined by interpolation from dose-response curves. All determinations were carried out in four to six separated experiments.

4.4. Determination of apoptosis by flow cytometry

Apoptosis and cell cycle profile were assessed by DNA fluorescence flow cytometry. HeLa cells treated with DMSO or tested compounds at indicated concentrations for 24 and 48 h were harvested, rinsed in PBS, resuspended and fixed in 80% ethanol, and stored at −20 °C in fixation buffer until ready for analysis. Then the pellets were suspended in 1 mL of fluorochromic solution (0.08 mg/mL PI (propidium iodide), 0.1% TritonX-100 and 0.2 mg/ml RNase A in 1× PBS) at room temperature in the dark for 30 min. The DNA content was analyzed by FACScan flow cytometer (Becton Dickinson, Mountain View, CA) and CELLQUEST software (Becton Dickinson). The population of apoptotic nuclei (subdiploid DNA peak in the DNA fluorescence histogram) was expressed as the percentage in the entire population.

4.5. Protein extraction and Western blotting

After the treatment of cells with vehicle (1% DMSO) or tested compounds for indicated time treatment, the cells were washed twice with PBS and reaction was terminated by the addition of 100 μL lysis buffer. For Western blot analysis, the amount of proteins (50 μg) were separated by electrophoresis in a 15% SDS–PAGE and transferred to a nitrocellulose membrane. After an overnight incubation at 4 °C in TBST/5% non-fat milk, the membrane was washed with TBST three times and immuno-reacted with the monocolonal primary antibodies, anti-poly-ADP-ribose polymerase(PARP) (1:500), anti-pro-caspase-3 (1:1000), anti-pro-caspase-9 (1:1000), anti-cleaved caspase-3 (1:1000), anti-phospho-ERK1/2 (1:1000), anti-ERK1/2 (1:1000), anti-phospho-p38 (1:1000), anti-p38 (1:1000), anti-phospho-c-Jun N-terminal kinase (1:500), anti-c-Jun N-terminal kinase (1:500), and anti-β-actin (1:1000) from Cell Signaling Technology (Beverly, MA) were used. After four washings with TBST, the anti-mouse or anti-rabbit IgG (dilute 1:10,000) was applied to the membranes for 1 h at room temperature. The membranes were washed with TBST for 1 h and the detection of signal was performed with an enhanced chemiluminescence (ECL) detection reagents.

4.6. Reactive oxygen species detection

Cells were assessed for the production of ROS using the dye, dihydroethidium (DHE).[13] DHE is a nonfluorescent, reduced form of ethidium that can passively cross plasma membranes of live cells. Cells were incubated with 5 μmol/L (Invitrogen, Carlsbad, CA) for 30 min, washed in PBS and visualized by light microscopy, using a Zeiss microscope with epifluorescence optics. Investigations were performed on four separate cultures, with replicates of two to six coverslips per culture analyzed.

Acknowledgments

Financial support from the National Science Council of the Republic of China (NSC 96-2113-M-032-007-MY2) and Tamkang University to A. Y. Shaw is gratefully acknowledged.

References and notes

1. Martindale, J. L.; Holbrook, N. J. *J. Cell Physiol.* **2002**, *192*, 1.
2. Manda, G.; Nechifor, M. T.; Neagu, T.-M. *Curr. Chem. Biol.* **2009**, *3*, 22.
3. Cherny, R. A.; Atwood, C. S.; Xilinas, M. E.; Gray, D. N.; Jones, W. D.; McLean, C. A.; Barnham, K. J.; Volitakis, I.; Fraser, F. W.; Kim, Y.; Huang, X.; Goldstein, L. E.; Moir, R. D.; Lim, J. T.; Beyreuther, K.; Zheng, H.; Tanzi, R. E.; Masters, C. L.; Bush, A. I. *Neuron* **2001**, *30*, 665.
4. Ritchie, C. W.; Bush, A. I.; Mackinnon, A.; Macfarlane, S.; Mastwyk, M.; MacGregor, L.; Kiers, L.; Cherny, R.; Li, Q. X.; Tammer, A.; Carrington, D.; Mavros, C.; Volitakis, I.; Xilinas, M.; Ames, D.; Davis, S.; Beyreuther, K.; Tanzi, R. E.; Masters, C. L. *Arch. Neurol.* **2003**, *60*, 1685.
5. Ding, W.-Q.; Liu, B.; Vaught, J. L.; Yamauchi, H.; Lind, S. E. *Cancer Res.* **2005**, *65*, 3389.
6. Ding, W.-Q.; Yu, H.-J.; Lind, S. E. *Cancer Lett.* **2008**, *271*, 251.
7. Chen, D.; Cui, Q. C.; Yang, H.; Barrea, R. A.; Sarkar, F. H.; Sheng, S.; Yan, B.; Reddy, G. P. V.; Dou, Q. P. *Cancer Res.* **2007**, *67*, 1636.
8. Burckhalter, J. H.; Leib, R. I. *J. Org. Chem.* **1961**, *26*, 4078.
9. Negm, N. A.; Morsy, S. M. I.; Said, M. M. *Bioorg. Med. Chem.* **2005**, *13*, 5921.
10. Shriner, R. L.; Grillot, G. F.; Teeters, W. O. *J. Am. Chem. Soc.* **1946**, *68*, 946.
11. Goodman, V. L.; Brewer, G. J.; Merajver, S. D. *Curr. Cancer Drug Targets* **2005**, *5*, 543.
12. Mattie, M. D.; McElwee, M. K.; Freedman, J. H. *J. Mol. Biol.* **2008**, *383*, 1008.
13. King, A.; Gottlieb, E.; Brooks, D. G.; Murphy, M. P.; Dunaief, J. L. *Photochem. Photobiol.* **2004**, *79*, 470.